NANO LETTERS

pubs.acs.org/NanoLett

Letter

Spontaneous Light Emission Assisted by Mie Resonances in Diamond Nanoparticles

Dmitry V. Obydennov, Daniil A. Shilkin, Ekaterina I. Elyas, Vitaly V. Yaroshenko, Oleg S. Kudryavtsev, Dmitry A. Zuev, Evgeny V. Lyubin, Evgeny A. Ekimov, Igor I. Vlasov, and Andrey A. Fedyanin*

Cite This: *Nano Lett.* 2021, 21, 10127–10132

Read Online

ACCESS | Metrics & More | Article Recommendations | Supporting Information

ABSTRACT: Spontaneous light emission is known to be affected by the local density of states and enhanced when coupled to a resonant cavity. Here, we report on an experimental study of silicon-vacancy (SiV) color center fluorescence and spontaneous Raman scattering from subwavelength diamond particles supporting low-order Mie resonances in the visible range. For the first time to our knowledge, we have measured the size dependences of the SiV fluorescence emission rate and the Raman scattering intensity from individual diamond particles in the range from 200 to 450 nm. The obtained dependences reveal a sequence of peaks, which we explicitly associate with specific multipole resonances. The results are in agreement with our theoretical analysis and highlight the potential of intrinsic optical resonances for developing nanodiamond-based lasers and single-photon sources.

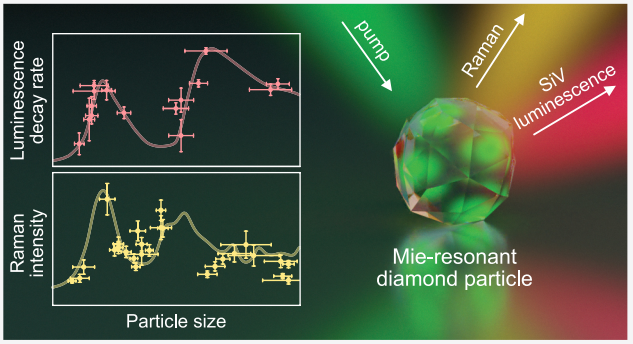

KEYWORDS: *nanodiamonds, Mie resonances, Purcell enhancement, silicon-vacancy centers*

INTRODUCTION

The ability to control spontaneous light emission is crucial for the development of quantum optics, advanced fluorescence, and Raman spectroscopy techniques.[1−3] Spontaneous Raman scattering and fluorescence efficiencies are known to be determined by the local density of photonic states and therefore depend on the environment. When coupled to a resonant cavity, spontaneous emission can be significantly enhanced. This phenomenon is often referred to as the Purcell effect and has been extensively used in a variety of applications ranging from generation of indistinguishable single photons[4] to ultrasensitive molecular imaging.[5]

Color centers in diamond are increasingly attractive fluorescent sources that have found numerous applications in biophotonics,[6−8] quantum optics,[9−12] and sensing.[13−15] Current fabrication techniques are capable of producing micro- and nanosized diamond particles with embedded color centers[16−18] as well as diamond films and wafers that can be tailored to create monolithic photonic structures with integrated sources.[19] For a number of applications such as biomarkers,[20] sensors,[21] and fiber-coupled single photon sources,[22] the use of separate crystals is either necessary or more convenient. Purcell enhancement of color-center emission has been repeatedly demonstrated for large-scale diamond resonant structures[23−25] and individual nanodiamonds coupled to external resonators.[26−28] Meanwhile, single diamond particles with a size of hundreds of nanometers exhibit low-order morphological resonances on their own,[29,30] the effect of which on the color center emission has only recently begun to be studied.

Morphology-dependent optical resonances are commonly referred to as Mie resonances due to their manifestation in the scattering spectra.[31−34] In high-permittivity particles, these resonances provide strong localization of electric and magnetic fields, which results in significant enhancement of nonlinear effects[35−39] and Raman response.[40−44] Coupling fluorescence to Mie-resonant structures allows one to modify the emission spectra[45,46] and to increase the spontaneous emission rate.[47] This has been experimentally demonstrated for quantum dots in Mie-resonant silicon structures[48] and fluorescent perovskite particles.[49]

A number of theoretical studies proposed to exploit Mie resonances in diamonds with embedded color centers for improvement of their radiative emission rate and collection efficiency.[50−52] Mie resonances in diamond particles have been a speculated cause of the experimentally observed variance in the measured excited state lifetime of chromium-[53] and

Received: July 5, 2021
Published: September 7, 2021

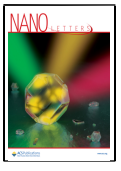

https://doi.org/10.1021/acs.nanolett.1c02616
Nano Lett. 2021, 21, 10127−10132

nitrogen-vacancy centers.[30] The modification of a single diamond particle has been shown to change the excited state lifetime of an embedded nitrogen-vacancy color center.[54] High-order Mie resonances of microsized diamonds have been experimentally demonstrated to modify the fluorescence emission spectrum.[55] However, the dependence of the color center emission rate on the hosting particle size has not been directly measured in the range of excitation of Mie resonances.

In this letter, we report on an experimental study of spontaneous light emission from Mie-resonant diamond particles containing multiple silicon-vacancy (SiV) color centers. For the first time to our knowledge, we examine the dependences of fluorescence emission rate and Raman scattering efficiency of submicron diamonds on the particle size and explicitly associate the observed enhancement peaks with specific low-order Mie resonances. We use a combination of numerical and analytical calculations to model the studied effects and discuss the importance of the obtained results for further research.

RESULTS AND DISCUSSION

An artistic schematic illustrating our experiments is shown in Figure 1. Single diamond particles are pumped using laser light

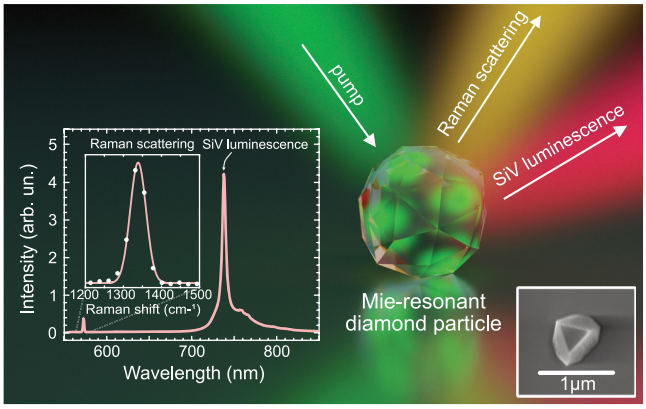

Figure 1. Schematic illustrating the concept of the study. The left inset shows a typical spectrum of the diamond emission. The inset in the right bottom corner is a scanning electron micrograph of a typical diamond particle under study.

at 532 nm. We measure the fluorescence emission rate and the Stokes Raman line intensity; the latter is then normalized by the particle volume. Depending on the diamond size and shape, Mie resonances can be excited at the frequency of the pump radiation, the color center luminescence, and the Raman emission line, resulting in different values being measured for different particles.

In this study, we used diamond particles containing multiple SiV centers; the latter are known for their bright luminescence with a narrow zero-phonon line and a weak phonon sideband.[56] The diamonds were synthesized by a high pressure high temperature (HPHT) technique from a mixture of Adamantane $C_{10}H_{16}$ and Tetraphenylsilane $C_{24}H_{20}Si$, and deposited on a glass substrate; see Supporting Information, Section I, for details of the fabrication process. As seen in the inset of Figure 1, the fabricated particles have a nonspherical shape; however, their fundamental optical resonances are well reproduced in the spherical shape approximation. The large number of color centers embedded in the particles and their orientation in different directions provide the overall fluorescence rate being determined primarily by the particle morphology instead of the position of individual emitters.

We started the experiments by characterizing the sample diamonds using scattering spectroscopy of individual particles; it was performed with a setup described elsewhere.[39] Typical scattering spectra obtained are shown in Figure 2a; the

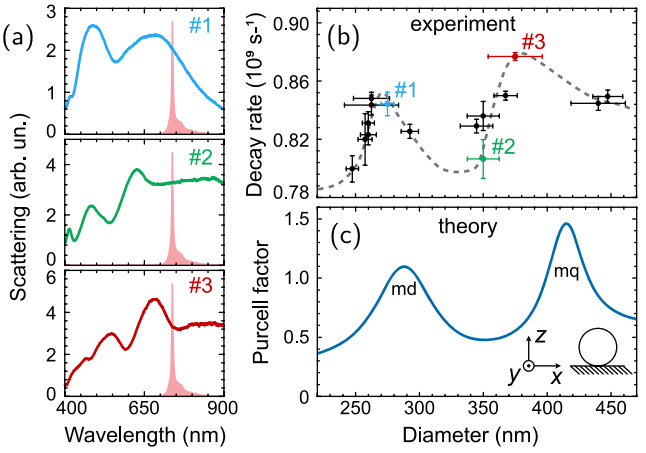

Figure 2. (a) Experimental scattering spectra (curves) of three diamond particles with the effective sizes of 275 ± 5 nm (#1), 350 ± 15 nm (#2), and 375 ± 20 nm (#3). The luminescence spectrum of SiV-centers is shown by the shaded areas. (b) Experimental decay rate for individual diamonds as a function of the effective diameter (dots). Colored dots denoted by numbers represent the particles whose scattering spectra are shown in (a). The gray dashed curve is a guide for the eyes. (c) Numerically calculated averaged Purcell factor at 738 nm for a diamond sphere on a glass substrate as a function of the sphere diameter. The inset shows the calculation geometry. Notations 'md' and 'mq' indicate the positions of the magnetic dipole and magnetic quadrupole resonances.

fluorescence spectrum is additionally indicated by shaded areas. One can see that depending on the chosen particle the fluorescence spectrally overlaps with various scattering resonances. To model the scattering, we performed finite-difference time-domain (FDTD) numerical simulations using the spherical-shape approximation taking into account the substrate presence and the experimental collection conditions; see Supporting Information, Section II for details of calculations. We then fitted the experimental spectra with the numerical ones using the sphere diameter and the overall scattering intensity as adjustable parameters. This allowed us to assign an effective size to each particle. Some of the particles have been visualized using scanning electron microscopy, and the ones with smaller effective sizes have been found to have smaller geometric dimensions; see Supporting Information, Section III, for details of the particle size analysis. We independently performed the scattering measurements for two orthogonal polarizations of the incident light and obtained two values of the effective size for each particle. In order to exclude strongly asymmetric diamonds, in further experiments we studied only particles with the obtained values differing by no more than 20 nm. Additionally, to identify the observed resonances, we performed analytical calculations using Mie theory for spherical particles in vacuum. According to our results, the observed scattering peaks correspond to the excitation of the magnetic dipole, quadrupole, and octupole modes. Electric-type Mie modes are excited as well; however,

https://doi.org/10.1021/acs.nanolett.1c02616
Nano Lett. 2021, 21, 10127−10132

the quality factor of the corresponding resonances is lower, and they do not reveal themselves as scattering peaks.[29]

In the next step, we directly measured the excited state lifetime using the time-correlated single photon counting (TCSPC) technique; see Supporting Information, Section IV, for details of the lifetime measurements. The experimental dependence of the fluorescence decay rate on the effective particle size is shown in Figure 2b. The maximum decay rate is observed for particles whose scattering peaks are close to the fluorescence one; the moderate discrepancy can be attributed to the maximum Purcell enhancement being typically shifted relative to the scattering maxima.[29] We performed a set of FDTD simulations to model the fluorescence rate variations and calculated the Purcell factor for an electric dipole emitting at 738 nm, embedded in a spherical particle on a glass substrate at the varied position and orientation of the dipole and the particle size; see Supporting Information, Section II, for details of the calculation procedure. The found Purcell factor values were then averaged as follows:

$$\langle F_{\mathrm{P}}\rangle \propto \frac{\sum_{j=x,y,z}\iiint_V I_j(\mathbf{r})F_{\mathrm{P}j}(\mathbf{r})d^3\mathbf{r}}{\sum_{j=x,y,z}\iiint_V I_j(\mathbf{r})d^3\mathbf{r}} \quad (1)$$

where $\mathbf{r}$ is the dipole position, V is the particle volume, $I_j(\mathbf{r})$ is the optical power directed to the collection optics, and $F_{\mathrm{P}j}(\mathbf{r})$ is the calculated Purcell factor value; the subscript $j = x, y, z$ denotes the dipole orientation along one of three axes. The weighting factor $I_j(\mathbf{r})$ was introduced to take into account the directivity of the emitters. Figure 2c demonstrates the resulted averaged Purcell factor at the fluorescence frequency as a function of the particle size. Both the experimental decay rate and numerical Purcell factor dependences have two pronounced maxima, which we associate with the excitation of the magnetic dipole and quadrupole Mie modes. In the experiment, we found that the total decay rate varies within 5%, while the calculated Purcell factor in the corresponding range changes at least 2-fold. This can be explained by the relatively low quantum yield of SiV centers.[56] Indeed, in the assumption that the quantum efficiency is 10%, the measured variance corresponds to an approximately 2-fold enhancement of the spontaneous emission rate. We expect that more significant variations in the total decay rate can be observed in the case of color centers with a higher quantum efficiency.

Further, we measured the intensity of the Raman Stokes line under continuous-wave excitation; see Supporting Information, Section V, for details of the Raman scattering measurements. The experimental dependence of the normalized Raman intensity on the particle size is shown in Figure 3a by dots. To understand this dependence theoretically, we introduced a model similar to that used in ref 57 and based on the following considerations. First, for each point of the crystal, the Raman scattering intensity is proportional to the Raman polarization, which is in turn proportional to the enhancement of the excitation light. Second, it is proportional to the local density of states (i.e., Purcell factor) at the Stokes frequency. We used FDTD simulations to model these processes under the experimental conditions of excitation and collection; see Supporting Information, Section II, for details of the calculations. The overall normalized Raman intensity was then found as follows:

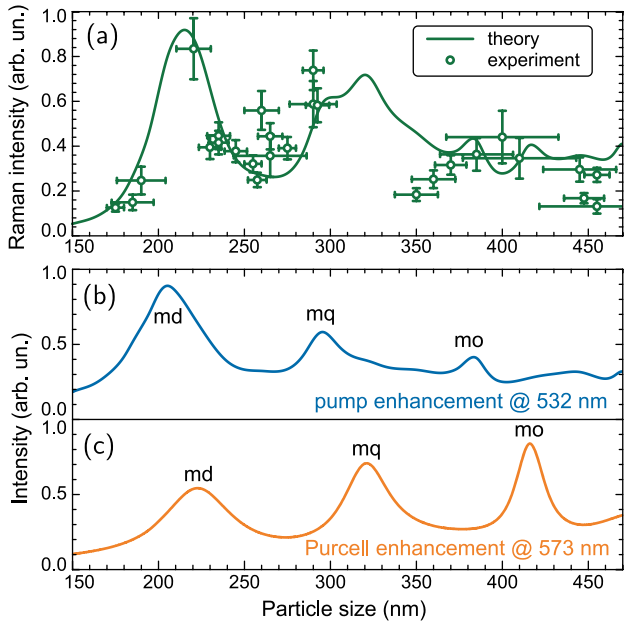

Figure 3. Raman response of individual diamond particles. (a) Experimental (dots) and theoretical (curve) Raman intensity normalized by the particle volume as a function of the particle size. (b) Calculated pump intensity enhancement under Gaussian beam excitation at 532 nm. (c) Calculated optical power emitted by an electric dipole at 573 nm and directed to the collection optics, averaged over the particle volume and polarization of the emitter. Notations 'md', 'mq', and 'mo' indicate the positions of the magnetic dipole, quadrupole, and octupole resonances, respectively.

$$\langle I_{\mathrm{Raman}}\rangle \propto \frac{1}{V}\sum_{j=x,y,z}\iiint_V |E(\mathbf{r})|^2|_{\lambda_{\mathrm{exc}}} I_j(\mathbf{r})|_{\lambda_{\mathrm{em}}} d^3\mathbf{r} \quad (2)$$

where $E(\mathbf{r})$ is the excitation electric field inside the particle at a wavelength of λ_{exc} = 532 nm and $I_j(\mathbf{r})$ is the optical power emitted by a dipole source at the Stokes wavelength λ_{em} = 573 nm and directed to the collection optics. The calculated dependence is shown in Figure 3a by the curve. It has a complex behavior explained by contributions from the two determining factors. To illustrate them independently, we plot the averaged pump field enhancement $\frac{1}{V}\iiint_V |E(\mathbf{r})|^2|_{\lambda_{\mathrm{exc}}} d^3\mathbf{r}$ in Figure 3b and the averaged collected emission power $\frac{1}{V}\sum_j \iiint_V I_j(\mathbf{r})|_{\lambda_{\mathrm{em}}} d^3\mathbf{r}$ in Figure 3c. An order-of-magnitude enhancement of the normalized Raman intensity is observed at the excitation of the magnetic dipole resonance at the pump wavelength. Note that our theoretical model does not account for the Raman polarizability being dependent on the crystal lattice orientation. This fact along with the nonsphericity of the particles limits the applicability of the model; however, both the variance percentage and overall behavior are in reasonable agreement with the theoretical results.

The results obtained demonstrate the importance of taking into account the excitation of Mie resonances when studying the emission from isolated diamond particles. By choosing particles of optimal size, one can significantly increase the color-center emission rate or the Raman scattering efficiency. Further improvement can be achieved by using diamonds of more regular shape. We expect that, eventually, Mie-resonant diamond particles can be used as Raman nanolasers[58] or

https://doi.org/10.1021/acs.nanolett.1c02616
Nano Lett. 2021, 21, 10127−10132

single-photon sources[50] with the emission rate and directionality determined by the particle morphology.

CONCLUSIONS

In summary, we have experimentally studied the effect of Mie resonances on the spontaneous light emission from subwavelength diamond particles. The observed decrease in the measured color-center luminescence lifetime at the excitation of the magnetic dipole and quadrupole modes corresponds to an approximately 2-fold increase of the spontaneous emission rate. An order-of-magnitude enhancement of the Stokes Raman scattering intensity is observed at the excitation of the magnetic dipole resonance. The results are in agreement with our theoretical analysis and highlight the potential of intrinsic optical resonances for developing nanodiamond-based lasers and single-photon sources.

ASSOCIATED CONTENT

Supporting Information

The Supporting Information is available free of charge at https://pubs.acs.org/doi/10.1021/acs.nanolett.1c02616.

Detailed description of the sample fabrication technique, numerical and analytical calculations, particle size analysis, fluorescence emission rate and Raman scattering measurements. (PDF)

AUTHOR INFORMATION

Corresponding Author

Andrey A. Fedyanin − *Faculty of Physics, Lomonosov Moscow State University, Moscow 119991, Russia;* orcid.org/0000-0003-4708-6895; Email: fedyanin@nanolab.phys.msu.ru

Authors

Dmitry V. Obydennov − *Faculty of Physics, Lomonosov Moscow State University, Moscow 119991, Russia*

Daniil A. Shilkin − *Faculty of Physics, Lomonosov Moscow State University, Moscow 119991, Russia;* orcid.org/0000-0001-7597-2734

Ekaterina I. Elyas − *Faculty of Physics, Lomonosov Moscow State University, Moscow 119991, Russia*

Vitaly V. Yaroshenko − *School of Physics and Engineering, ITMO University, St. Petersburg 191002, Russia;* orcid.org/0000-0003-2034-4962

Oleg S. Kudryavtsev − *Prokhorov General Physics Institute, Russian Academy of Sciences, Moscow 119991, Russia*

Dmitry A. Zuev − *School of Physics and Engineering, ITMO University, St. Petersburg 191002, Russia*

Evgeny V. Lyubin − *Faculty of Physics, Lomonosov Moscow State University, Moscow 119991, Russia*

Evgeny A. Ekimov − *Institute for High Pressure Physics, Russian Academy of Sciences, Troitsk 142190, Russia; Lebedev Physical Institute, Russian Academy of Sciences, Moscow 117924, Russia*

Igor I. Vlasov − *Prokhorov General Physics Institute, Russian Academy of Sciences, Moscow 119991, Russia*

Complete contact information is available at: https://pubs.acs.org/10.1021/acs.nanolett.1c02616

Notes

The authors declare no competing financial interest.

ACKNOWLEDGMENTS

The authors acknowledge stimulating discussions with Maxim Shcherbakov. This research was performed according to the MSU Development program of the Interdisciplinary Scientific and Educational School "Photonic and Quantum technologies. Digital medicine." D.V.O., D.A.S., E.I.E., and E.V.L. acknowledge support from the MSU Quantum Technology Center. Part of the research was supported by the Ministry of Science and Higher Education of the Russian Federation (Contract No. 14.W03.31.0008, spectroscopy measurements) and the Russian Science Foundation (Grant No. 20-12-00371, numerical simulations; Grant No. 19-12-00407, synthesis, preparation and characterization of the diamond sample).

REFERENCES

(1) Eisaman, M. D.; Fan, J.; Migdall, A.; Polyakov, S. V. Invited review article: Single-photon sources and detectors. *Rev. Sci. Instrum.* **2011**, *82*, 071101.

(2) Becker, W. Fluorescence lifetime imaging−techniques and applications. *J. Microsc.* **2012**, *247*, 119−136.

(3) Wang, P.; Chen, W.; Wan, F.; Wang, J.; Hu, J. A review of cavity-enhanced Raman spectroscopy as a gas sensing method. *Appl. Spectrosc. Rev.* **2020**, *55*, 393−417.

(4) Liu, F.; Brash, A. J.; O'Hara, J.; Martins, L. M. P. P.; Phillips, C. L.; Coles, R. J.; Royall, B.; Clarke, E.; Bentham, C.; Prtljaga, N.; Itskevich, I. E.; Wilson, L. R.; Skolnick, M. S.; Fox, A. M. High Purcell factor generation of indistinguishable on-chip single photons. *Nat. Nanotechnol.* **2018**, *13*, 835−840.

(5) Hümmer, T.; Noe, J.; Hofmann, M. S.; Hänsch, T. W.; Högele, A.; Hunger, D. Cavity-enhanced Raman microscopy of individual carbon nanotubes. *Nat. Commun.* **2016**, *7*, 12155.

(6) Faklaris, O.; Joshi, V.; Irinopoulou, T.; Tauc, P.; Sennour, M.; Girard, H.; Gesset, C.; Arnault, J.-C.; Thorel, A.; Boudou, J.-P.; Curmi, P. A.; Treussart, F. Photoluminescent diamond nanoparticles for cell labeling: study of the uptake mechanism in mammalian cells. *ACS Nano* **2009**, *3*, 3955−3962.

(7) Chang, B.-M.; Lin, H.-H.; Su, L.-J.; Lin, W.-D.; Lin, R.-J.; Tzeng, Y.-K.; Lee, R. T.; Lee, Y. C.; Yu, A. L.; Chang, H.-C. Highly fluorescent nanodiamonds protein-functionalized for cell labeling and targeting. *Adv. Funct. Mater.* **2013**, *23*, 5737−5745.

(8) Chen, X.; Zhang, W. Diamond nanostructures for drug delivery, bioimaging, and biosensing. *Chem. Soc. Rev.* **2017**, *46*, 734−760.

(9) Sipahigil, A.; et al. An integrated diamond nanophotonics platform for quantum-optical networks. *Science* **2016**, *354*, 847−850.

(10) Schröder, T.; Mouradian, S. L.; Zheng, J.; Trusheim, M. E.; Walsh, M.; Chen, E. H.; Li, L.; Bayn, I.; Englund, D. Quantum nanophotonics in diamond. *J. Opt. Soc. Am. B* **2016**, *33*, B65−B83.

(11) Bhaskar, M. K.; Sukachev, D. D.; Sipahigil, A.; Evans, R. E.; Burek, M. J.; Nguyen, C. T.; Rogers, L. J.; Siyushev, P.; Metsch, M. H.; Park, H.; Jelezko, F.; Lončar, M.; Lukin, M. D. Quantum nonlinear optics with a germanium-vacancy color center in a nanoscale diamond waveguide. *Phys. Rev. Lett.* **2017**, *118*, 223603.

(12) Bradac, C.; Gao, W.; Forneris, J.; Trusheim, M. E.; Aharonovich, I. Quantum nanophotonics with group IV defects in diamond. *Nat. Commun.* **2019**, *10*, 5625.

(13) Maze, J. R.; Stanwix, P. L.; Hodges, J. S.; Hong, S.; Taylor, J. M.; Cappellaro, P.; Jiang, L.; Dutt, M. V. G.; Togan, E.; Zibrov, A. S.; Yacoby, A.; Walsworth, R. L.; Lukin, M. D. Nanoscale magnetic sensing with an individual electronic spin in diamond. *Nature* **2008**, *455*, 644−647.

(14) Ermakova, A.; Pramanik, G.; Cai, J. M.; Algara-Siller, G.; Kaiser, U.; Weil, T.; Tzeng, Y. K.; Chang, H. C.; McGuinness, L. P.; Plenio, M. B.; Naydenov, B.; Jelezko, F. Detection of a few metallo-protein molecules using color centers in nanodiamonds. *Nano Lett.* **2013**, *13*, 3305−3309.

(15) Tzeng, Y.-K.; Tsai, P.-C.; Liu, H.-Y.; Chen, O. Y.; Hsu, H.; Yee, F.-G.; Chang, M.-S.; Chang, H.-C. Time-resolved luminescence

nanothermometry with nitrogen-vacancy centers in nanodiamonds. *Nano Lett.* **2015**, *15*, 3945−3952.
(16) Vlasov, I. I.; et al. Molecular-sized fluorescent nanodiamonds. *Nat. Nanotechnol.* **2014**, *9*, 54−58.
(17) Andrich, P.; Alemán, B. J.; Lee, J. C.; Ohno, K.; de las Casas, C. F.; Heremans, F. J.; Hu, E. L.; Awschalom, D. D. Engineered micro- and nanoscale diamonds as mobile probes for high-resolution sensing in fluid. *Nano Lett.* **2014**, *14*, 4959−4964.
(18) Grudinkin, S. A.; Feoktistov, N. A.; Bogdanov, K. V.; Baranov, M. A.; Baranov, A. V.; Fedorov, A. V.; Golubev, V. G. Chemical vapor deposition of isolated spherical diamond particles with embedded silicon-vacancy color centers onto the surface of synthetic opal. *Semiconductors* **2014**, *48*, 268−271.
(19) Aharonovich, I.; Greentree, A. D.; Prawer, S. Diamond photonics. *Nat. Photonics* **2011**, *5*, 397−405.
(20) Fu, C.-C.; Lee, H.-Y.; Chen, K.; Lim, T.-S.; Wu, H.-Y.; Lin, P.-K.; Wei, P.-K.; Tsao, P.-H.; Chang, H.-C.; Fann, W. Characterization and application of single fluorescent nanodiamonds as cellular biomarkers. *Proc. Natl. Acad. Sci. U. S. A.* **2007**, *104*, 727−732.
(21) Fan, J.-W.; Cojocaru, I.; Becker, J.; Fedotov, I. V.; Alkahtani, M. H. A.; Alajlan, A.; Blakley, S.; Rezaee, M.; Lyamkina, A.; Palyanov, Y. N.; Borzdov, Y. M.; Yang, Y.-P.; Zheltikov, A.; Hemmer, P.; Akimov, A. V. Germanium-vacancy color center in diamond as a temperature sensor. *ACS Photonics* **2018**, *5*, 765−770.
(22) Schröder, T.; Schell, A. W.; Kewes, G.; Aichele, T.; Benson, O. Fiber-integrated diamond-based single photon source. *Nano Lett.* **2011**, *11*, 198−202.
(23) Hausmann, B. J. M.; Shields, B. J.; Quan, Q.; Chu, Y.; de Leon, N. P.; Evans, R.; Burek, M. J.; Zibrov, A. S.; Markham, M.; Twitchen, D. J.; Park, H.; Lukin, M. D.; Loncăr, M. Coupling of NV centers to photonic crystal nanobeams in diamond. *Nano Lett.* **2013**, *13*, 5791−5796.
(24) Riedrich-Möller, J.; Arend, C.; Pauly, C.; Mücklich, F.; Fischer, M.; Gsell, S.; Schreck, M.; Becher, C. Deterministic coupling of a single silicon-vacancy color center to a photonic crystal cavity in diamond. *Nano Lett.* **2014**, *14*, 5281−5287.
(25) Zhang, J. L.; Sun, S.; Burek, M. J.; Dory, C.; Tzeng, Y.-K.; Fischer, K. A.; Kelaita, Y.; Lagoudakis, K. G.; Radulaski, M.; Shen, Z.-X.; Melosh, N. A.; Chu, S.; Lončar, M.; Vučković, J. Strongly cavity-enhanced spontaneous emission from silicon-vacancy centers in diamond. *Nano Lett.* **2018**, *18*, 1360−1365.
(26) Kumar, S.; Huck, A.; Andersen, U. L. Efficient coupling of a single diamond color center to propagating plasmonic gap modes. *Nano Lett.* **2013**, *13*, 1221−1225.
(27) Kaupp, H.; Hümmer, T.; Mader, M.; Schlederer, B.; Benedikter, J.; Haeusser, P.; Chang, H.-C.; Fedder, H.; Hänsch, T. W.; Hunger, D. Purcell-enhanced single-photon emission from nitrogen-vacancy centers coupled to a tunable microcavity. *Phys. Rev. Appl.* **2016**, *6*, 054010.
(28) Bogdanov, S. I.; Shalaginov, M. Y.; Lagutchev, A. S.; Chiang, C.-C.; Shah, D.; Baburin, A. S.; Ryzhikov, I. A.; Rodionov, I. A.; Kildishev, A. V.; Boltasseva, A.; Shalaev, V. M. Ultrabright room-temperature sub-nanosecond emission from single nitrogen-vacancy centers coupled to nanopatch antennas. *Nano Lett.* **2018**, *18*, 4837−4844.
(29) Shilkin, D. A.; Shcherbakov, M. R.; Lyubin, E. V.; Katamadze, K. G.; Kudryavtsev, O. S.; Sedov, V. S.; Vlasov, I. I.; Fedyanin, A. A. Optical magnetism and fundamental modes of nanodiamonds. *ACS Photonics* **2017**, *4*, 1153−1158.
(30) Zalogina, A. S.; Savelev, R. S.; Ushakova, E. V.; Zograf, G. P.; Komissarenko, F. E.; Milichko, V. A.; Makarov, S. V.; Zuev, D. A.; Shadrivov, I. V. Purcell effect in active diamond nanoantennas. *Nanoscale* **2018**, *10*, 8721−8727.
(31) Kuznetsov, A. I.; Miroshnichenko, A. E.; Fu, Y. H.; Zhang, J.; Luk'yanchuk, B. *Sci. Rep.* **2012**, *2*, 492.
(32) Evlyukhin, A. B.; Novikov, S. M.; Zywietz, U.; Eriksen, R.; Reinhardt, C.; Bozhevolnyi, S. I.; Chichkov, B. N. Demonstration of magnetic dipole resonances of dielectric nanospheres in the visible region. *Nano Lett.* **2012**, *12*, 3749−3755.
(33) Kivshar, Y.; Miroshnichenko, A. Meta-optics with Mie resonances. *Opt. Photonics News* **2017**, *28*, 24−31.
(34) Shilkin, D. A.; Lyubin, E. V.; Shcherbakov, M. R.; Lapine, M.; Fedyanin, A. A. Directional optical sorting of silicon nanoparticles. *ACS Photonics* **2017**, *4*, 2312−2319.
(35) Shcherbakov, M. R.; Neshev, D. N.; Hopkins, B.; Shorokhov, A. S.; Staude, I.; Melik-Gaykazyan, E. V.; Decker, M.; Ezhov, A. A.; Miroshnichenko, A. E.; Brener, I.; Fedyanin, A. A.; Kivshar, Y. S. Enhanced third-harmonic generation in silicon nanoparticles driven by magnetic response. *Nano Lett.* **2014**, *14*, 6488−6492.
(36) Timpu, F.; Sergeyev, A.; Hendricks, N. R.; Grange, R. Second-harmonic enhancement with Mie resonances in perovskite nanoparticles. *ACS Photonics* **2017**, *4*, 76−84.
(37) Zhang, C.; Xu, Y.; Liu, J.; Li, J.; Xiang, J.; Li, H.; Li, J.; Dai, Q.; Lan, S.; Miroshnichenko, A. E. Lighting up silicon nanoparticles with Mie resonances. *Nat. Commun.* **2018**, *9*, 2964.
(38) Kroychuk, M. K.; Yagudin, D. F.; Shorokhov, A. S.; Smirnova, D. A.; Volkovskaya, I. I.; Shcherbakov, M. R.; Shvets, G.; Kivshar, Y. S.; Fedyanin, A. A. Tailored nonlinear anisotropy in Mie-resonant dielectric oligomers. *Adv. Opt. Mater.* **2019**, *7*, 1900447.
(39) Kroychuk, M. K.; Shorokhov, A. S.; Yagudin, D. F.; Shilkin, D. A.; Smirnova, D. A.; Volkovskaya, I.; Shcherbakov, M. R.; Shvets, G.; Fedyanin, A. A. Enhanced nonlinear light generation in oligomers of silicon nanoparticles under vector beam illumination. *Nano Lett.* **2020**, *20*, 3471−3477.
(40) Murphy, D. V.; Brueck, S. R. J. Enhanced Raman scattering from silicon microstructures. *Opt. Lett.* **1983**, *8*, 494−496.
(41) Bezares, F. J.; Long, J. P.; Glembocki, O. J.; Guo, J.; Rendell, R. W.; Kasica, R.; Shirey, L.; Owrutsky, J. C.; Caldwell, J. D. Mie resonance-enhanced light absorption in periodic silicon nanopillar arrays. *Opt. Express* **2013**, *21*, 27587−27601.
(42) Dmitriev, P. A.; Baranov, D. G.; Milichko, V. A.; Makarov, S. V.; Mukhin, I. S.; Samusev, A. K.; Krasnok, A. E.; Belov, P. A.; Kivshar, Y. S. Resonant Raman scattering from silicon nanoparticles enhanced by magnetic response. *Nanoscale* **2016**, *8*, 9721−9726.
(43) Zograf, G.; Baryshnikova, K.; Petrov, M.; Makarov, S. Enhanced Raman scattering for probing near-field distribution in all-dielectric nanostructures. *Adv. Photonics Res.* **2021**, *2*, 2000139.
(44) Matthiae, M.; Nielsen, K. E. S.; Larroche, A.; Zhou, C.; Kristensen, A.; Raza, S. Probing optical resonances of silicon nanostructures using tunable-excitation Raman spectroscopy. *Opt. Express* **2019**, *27*, 38479−38492.
(45) Owen, J. F.; Chang, R. K.; Barber, P. W. Morphology−dependent resonances in Raman scattering, fluorescence emission, and elastic scattering from microparticles. *Aerosol Sci. Technol.* **1982**, *1*, 293−302.
(46) Staude, I.; Khardikov, V. V.; Fofang, N. T.; Liu, S.; Decker, M.; Neshev, D. N.; Luk, T. S.; Brener, I.; Kivshar, Y. S. Shaping photoluminescence spectra with magnetoelectric resonances in all-dielectric nanoparticles. *ACS Photonics* **2015**, *2*, 172−177.
(47) Zambrana-Puyalto, X.; Bonod, N. Purcell factor of spherical Mie resonators. *Phys. Rev. B: Condens. Matter Mater. Phys.* **2015**, *91*, 195422.
(48) Rutckaia, V.; Heyroth, F.; Novikov, A.; Shaleev, M.; Petrov, M.; Schilling, J. Quantum dot emission driven by Mie resonances in silicon nanostructures. *Nano Lett.* **2017**, *17*, 6886−6892.
(49) Tiguntseva, E. Y.; Zograf, G. P.; Komissarenko, F. E.; Zuev, D. A.; Zakhidov, A. A.; Makarov, S. V.; Kivshar, Y. S. Light-emitting halide perovskite nanoantennas. *Nano Lett.* **2018**, *18*, 1185−1190.
(50) Greffet, J. J.; Hugonin, J. P.; Besbes, M.; Lai, N. D.; Treussart, F.; Roch, J. F. *Diamond particles as nanoantennas for nitrogen-vacancy color centers*. 2011, arXiv:1107.0502 [physics.optics]. arXiv.org e-Print archive. https://arxiv.org/abs/1107.0502 (accessed Aug 30, 2021).
(51) Shugayev, R.; Bermel, P. Core-shell Mie resonant structures for quantum computing applications. *Appl. Phys. Lett.* **2016**, *109*, 221102.
(52) Hong, H.-G.; Lee, S.-B.; Heo, M.-S.; Park, S. E.; Kwon, T. Y. Mie resonance-enhanced pumping and detection efficiency for shallow nitrogen-vacancy centers in diamond. *Opt. Express* **2016**, *24*, 28815−28828.

https://doi.org/10.1021/acs.nanolett.1c02616
Nano Lett. 2021, 21, 10127−10132

(53) Castelletto, S.; Boretti, A. Radiative and nonradiative decay rates in chromium-related centers in nanodiamonds. *Opt. Lett.* **2011**, *36*, 4224−4226.
(54) Inam, F. A.; Steel, M. J.; Castelletto, S. Effects of the hosting nano-environment modifications on NV centres fluorescence emission. *Diamond Relat. Mater.* **2014**, *45*, 64−69.
(55) Grudinkin, S. A.; Perova, T. S.; Moore, R. A.; Rakovich, Y. P.; Golubev, V. G.; Feoktistov, N. A. Whispering gallery modes from CVD diamond spherical-like particles. *Opt. Mater.* **2007**, *29*, 983−986.
(56) Neu, E.; Agio, M.; Becher, C. Photophysics of single silicon vacancy centers in diamond: implications for single photon emission. *Opt. Express* **2012**, *20*, 19956−19971.
(57) Frizyuk, K.; Hasan, M.; Krasnok, A.; Alú, A.; Petrov, M. Enhancement of Raman scattering in dielectric nanostructures with electric and magnetic Mie resonances. *Phys. Rev. B: Condens. Matter Mater. Phys.* **2018**, *97*, 085414.
(58) Kim, K.-H.; Choe, S.-H. Proposal for ultrasmall deep ultraviolet diamond Raman nanolaser. *Appl. Phys. B: Lasers Opt.* **2016**, *122*, 263.

https://doi.org/10.1021/acs.nanolett.1c02616
Nano Lett. 2021, 21, 10127−10132